1 Background and Masking System

1.1 Introduction

Three types of background problems have to be considered for the experiment at JLC-I. They are (a) high energy muons that are produced through electromagnetic interactions between the incoming beam and collimating materials in the upstream collimation section, (b) synchrotron radiations emitted by the beam when it traverses through the beam line magnets, particularly the final focus lens, and (c) e^+e^- pairs created in beam-beam collision at interaction point(IP).

Collision parameters are optimized to minimize these backgrounds while a luminosity is kept to be maximal value. The masking system in the interaction region is carefully designed to minimize such e^+e^- pair background and synchrotron radiation photons. We developed a design where the photons would not enter the active detector volume unless they are emitted by electrons/positrons beyond transverse offsets of $\pm 6\sigma_x$ or $\pm 35\sigma_y$ which are the nominal values of our collimation scheme. Here the σ_x and σ_y denote the size of the design emittance beam. In this calculation the beam is assumed to have a bi-Gaussian transverse distribution up to $\pm 3\sigma_{x(y)}$, followed by a 1 % flat tail beyond it.

Should synchrotron radiation backgrounds turn out be unacceptably large in the real life, two possibilities have to be examined: (1) the core emittance of the beam is too large, or (2) the lateral tail spread of the beam is too large. In case of (1), if the emittance cannot be rapidly improved, the experiment may be run by increasing $\beta^\star$, thus by reducing the lateral spread of synchrotron radiations at IP. In case of (2), if the reduction of beam tails turns out to be difficult, we need to resort to some beam collimation. It should be pointed out that the causes (1) and (2) are likely to occur (if they do) simultaneously. Hence the counter measures will have to be a combination of emittance improvement, optics retuning, beam tail reduction, beam collimation and others.

With beam collimation with metalic slits we create a possibility of high energy muon productions. Such muons can travel along the downstream beam line and penetrate the detector longitudinally, leaving huge energy deposits in the calorimeter and elesewhere. They can cause serious problems in the trigger and data analysis. The flux of muons depends on the tightness of the collimation as well as presence of downstream beam line components. For this reason an excessive beam collimation could turn out to be counter-productive. It should be used with a care, to reduce production of secondary tails off the collimation materials as well as to avoid an emittance growth due to collimator wake fields.

In subsequent sections we describe our strategies on how to handle those backgrounds.

1.2 Muons

It is difficult to estimate how many muons will be created in the collimation section since we do not know the mechanism to create a beam tail. Of cource there is no muon background problem with no tail, *i.e.* gaussian beam. Total number of muons(N_μ) per electron are calculated as a function of incident electron energy(E_e) by MUON89[1] code and it is approximately expressed as,

$$N_\mu = 3.9(2.3) \cdot 10^{-4} \cdot E_e(\mathrm{GeV})/250 \quad \text{for} \quad \mathrm{E}_\mu > 2(5)\mathrm{GeV}. \tag{1}$$

The muons may be created as many as $2.8(1.7) \cdot 10^6$ because of $N_\mu \cdot 72$ (bunches/train) $\cdot$ 10^{10} (e's/bunch)$\cdot 10^{-2}$(1% tail). Typical scattering angle of muon (θ_μ) is m_μ / E_μ, *i.e.* $\theta_\mu =$ 1 mrad for $E_\mu = 100$ GeV. Since a distance between a collimator and IP is about 1 km, these muons are spread over detector. Low energy muons($E_\mu <$ a few GeV) can be easily absorbed in concrete of 10 m thickness. In order to control them JLC-I has a collimation section in the final focus system. It comprizes a collimator(30 radiation length), a muon attenuator[2] and "big bending" magnet(~ 15 mrad).

The penetrating probability after a collimator is mainly come from an edge scattering and it has been calculated to be 10^{-4} by R.Nelson[4]. Our collimation scheme employs "twice" collimation, that is, the beam is collimated twice at least in its phase space(x, x', y, y' and energy). Therefore no sizable tail is expected downstream the collimation section. The probability of repopulation in a tail is also estimated to be $10^{-7}/n^2$ per 1km beam line with the vacuum of 10^{-10} torr, where n is the position ($n\sigma_{x(y)}$) of the repopulation, provided that the repopulation is due to Coulomb scattering between electron/positron and residual gas ion(CO)[5]. In our case of $\pm 6\sigma_x$ of the collimation and about 1km between the collimation and IP, the probability is less than $3 \cdot 10^{-9}$. The corresponding number of particles in the tails is $3 \cdot 10^3$/train at most , wihch is acceptable. The detailed description of the collimation section is found in "Final Focus System" of this proposal. It should be stressed that high vacuum ($< 10^{-10}$ torr) is highly desired in final focus system in order to avoid scatterings of tail particles at QC1 pole tips *etc.* as well as synchrotron radiations .

The principle idea of muon attenuation is to confine muons inside iron pipe which has two axial magnetic fields of 1 Tesla in opposite directions corresponding to μ^+'s and μ^-'s, then simultaneously absorb muons[3]. The length of the muon attenuator is mainly determined by muon ranges and it is about 100 m at most, where muon range in iron is 56(98) m for E_μ=100(200) GeV[6]. With this scheme there is expected to be negligibly small number of muons at IP.

1.3 Synchrotron Radiations

A. Last Bending Magnet

Since the last bending magnet is located at 117.4 m from IP and its total bending angle is 0.55 mrad, synchrotron radiations are horizontally spread up to 6.4 cm at IP. The critical energy is about 1 MeV and the intensity is almost same as the beam intensity (O(10^{12})/train). As a half aperture of final quadrupole magnet QC1 is 0.67 cm, it is necessary to shield the synchrotron radiations. For this purpose a mask is installed at 61 m from the last bending magnet, near QC3. The mask can be made by 21cm long tungsten which corresponds to 20λ ($2 \cdot 10^{-9}$ attenuation) for a few MeV photons. Since its minimum (half) aperture is 0.3 cm in horizontal and vertical directions, which correspond to $22\sigma_x$ and $264\sigma_y$, respectively, there is no emittance growth due to a wake field by the mask. There is no secondary particles ($e^\pm$'s and $\mu^\pm$'s) created at the mask because no beam tail can hit it. With this mask the synchrotron radiation is well collimated to 1 cm at IP.

B. Quadrupole Magnets

There are only 4 quadrupole magnets, QC1 - QC4, in a straight section between the last bending magnet and IP. Among them QC2 is the largest radiation source. Here we do not consider any mask since a doublet of final quadrupole magnets (QC1 and QC2) is so near IP that there is no way to stop back-scattered synchrotron radiations from the mask. The control of synchrotron radiations from the quadrupole magnets is uniquely provided by the

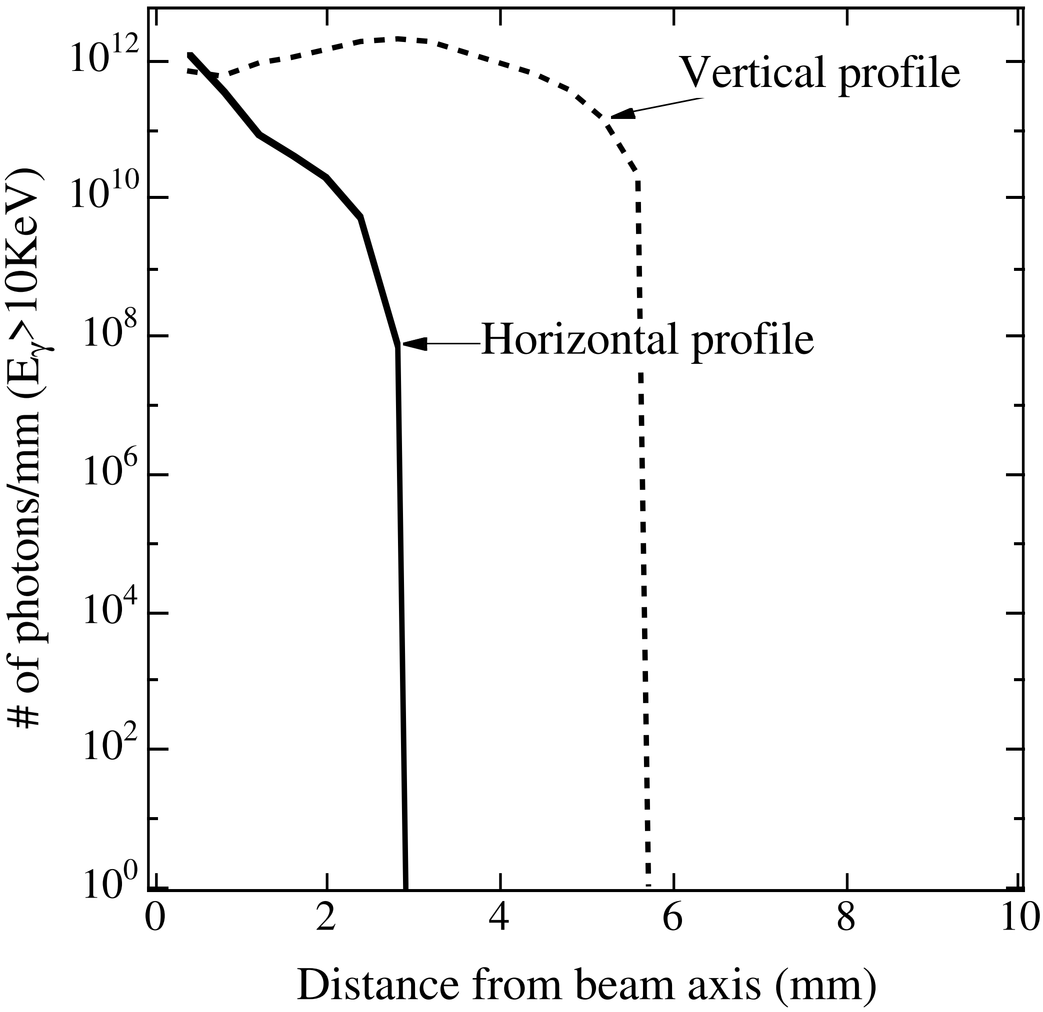

Figure 1: Profile of synchrotron radiation per train crossing from QC4-QC1 at the front face of QC1 seen from IP,*i.e.* 2.5m upstream from IP for E_{beam} =250GeV.

optics of the final focus system. The optics is carefully determined in order to have a large bore (1.34 cm ϕ) of QC1, which is enough for the synchrotron radiations to go through without scattering for the beam collimated at $\pm 6\sigma_x$, $\pm 35\sigma_y$. The tail of the synchrotron radiations is also produced by the tail of beam. Figure 1 shows the lateral spread of radiations from QC3,QC4,QC2 and QC1 itself in front face of QC1, *i.e.* 2.5 m upstream of IP. Tolerable number of photons is $O(10^7)$ for x,y $>$ 0.67cm in this figure, which may hit the "iron" pole of QC1 and back-scatter into IP. As discussed in the previous section there must be tails up to 10^4 photons beyond sharp cuts of the lateral spreads in Fig.1. We show Fig.2 to see how the radiations go through QC1. In Fig.2 cross sectional views of radiations are shown at the entrance and the exit of QC1. The two off-axis profiles are those of the radiations with exit beam (after collision) since a crossing angle is 8 mrad at E_{beam} =250GeV and QC1 is 2.4 m long, whereas the profile at the center is that of focusing beam (before collision). Therefore there is no serious background problem of the synchrotron radiations.

Figure 2: Cross sectional views of incoming and outgoing synchrotron radiations, which are shown as ellipses, at the entrance and exit of QC1, for E_{beam}=250GeV, where the crossing angle of two beams is 8 mrad. QC1 is located at 2.5m upstream from IP, and its half aperture and length are 6.7mm and 2.4m, respectively. Its coils are indicated by crosses boxes. Disrupted beams after collision are also plotted by dots.

1.4 e^+e^- pairs

e^+e^- pairs are created in coherent[7] and incoherent processes at linear colliders. The coherent process is the beamstrahlung photon conversion by a strongly collective magnetic field produced by the opposing beam. Its probability depends mainly on a beamstrahlung parameter(Υ). Since the condition of $\Upsilon \sim 1$ corresponds to a threshold for a photon of beam energy to convert into an e^+e^- pair in the magnetic field and the pair creation with $\Upsilon < 1$ is exponentially supressed as $\exp(-16/8\Upsilon)$, coherent pairs is only relevant at a linear collider with $\Upsilon \geq 1$. For JLC-I the number of coherent pairs are negligibly small because of $\Upsilon = 0.093(0.19)$ at E_{beam}=150(250) GeV. On the contrary, the incoherent process comprising (a) BW (Breit-Wheeler): $\gamma\gamma \rightarrow e^+e^-$, (b)BH (Bethe-Heitler): $\gamma e^\pm \rightarrow e^\pm e^+e^-$, and (c)LL (Landau-Lifshits): $e^+e^- \rightarrow e^+e^-e^+e^-$ has no such energy threshold and it is proportional to luminosity, where γ is a beamstrahlung photon, and its number is about one per a beam particle for JLC-I. Their typical cross sections are (a)BW: $1.9 \cdot 10^{-27}\mathrm{cm}^2$, (b)BH: $2.2 \cdot 10^{-25}\mathrm{cm}^2$ and (c)LL: $4.5 \cdot 10^{-26}\mathrm{cm}^2$ at E_{beam}=250 GeV. As luminosity per bunch crossing is very high, which is $1.0 \cdot 10^{30}\mathrm{cm}^{-2}\mathrm{bunch}^{-1}$ at E_{beam}=250 GeV, enormous number of pairs are created at each collision, then they may kill an experiment.

The backgrounds of the pairs can be classified in two ways, *i.e.* (i) primary and (ii) secondary background. The former comprizes pairs which directly enter a detector region, then overlap a physics signal. The most affective region of a detetor is for a vertex detector because of the small transverse momenta of the pairs. The latter comprizes secondary particles,*i.e.* neutrons and photons, which are created in a collision between the pairs and a pole tip of QC1. The number of neutrons(N_n) is proportional to the total deposit energy of the pairs (ΣE_e), *i.e.* $N_n \sim 0.13 \cdot \Sigma E_e$, while the number of photons(N_γ) is proportional to the total number of the pairs (ΣN_e), *i.e.* $N_\gamma \sim \Sigma N_e$. To quantatively estimate these backgrounds we simulate the pairs by ABEL. For the generation of the pairs ABEL takes account of inherent scattering angles of the pairs, which can be larger than their characteristic angles of m_e/E_e, a geometric reduction due to smaller beam spot size (especially in vertical direction) than the typical impact parameters and an effect of strong external field. In ABEL the pairs are kicked by the strong electromagnetic field produced by the opposing beam, then they can acquire larger transverse momenta than the inherent ones. The final scattering angle (θ_e) is the sum of the inherent angle (θ_e°) and kick angle (θ_{kick}). The detailed description of this simulation is found elsewhere[8].

Figure 3 shows a scatter plot of the pairs in a plane of the final scattering angle (horizontal axis) and the transverse momentum (vetical axis). A sharp boundary is clearly seen in this figure, which corresponds to the maximum kick angle of the pairs ($\theta_e^\circ << \theta_{kick}$), and the pairs are seen to be also largely scattered beyound this boundary ($\theta_e^\circ >> \theta_{kick}$). The pairs in very forward angular region ($\theta_e < 0.15$) hit QC1 *etc.* , then the secondary photons are back-scattered. For further study of the primary background we plot the pairs of $\theta_e > 0.15$ (outside of a mask which is described in next section) as a function of their transverse momenta in Fig.4. The results are listed in Tab.1 for all cases of JLC-I at E_{beam}=150 and 250 GeV together with machine parameters relevant to background study. From ΣE_e's in Tab.1 the total number of neutrons is $O(10^6)$ per train crossing. Typical energy deposit of a neutron is estimated to be about 0.1 MeV, which is normalized to electron energy, with a detection efficiency of $< 50\%$ in our calorimeters[9]. Assuming the neutrons spread uniformly over 20k channel calorimeter, energy deposit per channel is a few MeV, *i.e.* $10^6 \cdot 0.1(\mathrm{MeV}) \cdot 0.5(\mathrm{eff.})/(2 \cdot 10^4)$. The other detector is less sensitive to neutrons. Therefore the neutrons cause no serious problem. Possible problems of

Figure 3: Pairs simulated by ABEL on a plane of p_t and θ_e at E_{beam}=250GeV for JLC-I(c-band).

secondary photons and backgrounds in a vertex detector will be discussed in sebsequent sections.

1.5 Masking System

Our masking system is schematically shown in Fig.5. A mask is employed in order to shield against the large amount of the secondary photons. The probability for the O(10^7) photons/train (see Tab.1) to escape from the mask, η_{mask}, should be less than 10^{-3}, which is geometrically determined by the front aperture of the mask. Most of the escaped photons hit the mask surface on the opposite side, then they enter the detector region. In addition the mask must have enough thickness to absorb the photons, that is, its attenuation coefficient should be less than 10^{-5} for 0.5MeV photons which corresponds to a 5cm thick tungsten. We require that the acceptable number of photons in the detector region is O(10^2) per train crossing. As we fix the angular region of the mask as $0.15 < \theta_{mask} < 0.2$, it remains to determine only one parameter to fully specify the geometry of the mask. We take the half aperture of the mask, R_{mask} in Fig.5, for

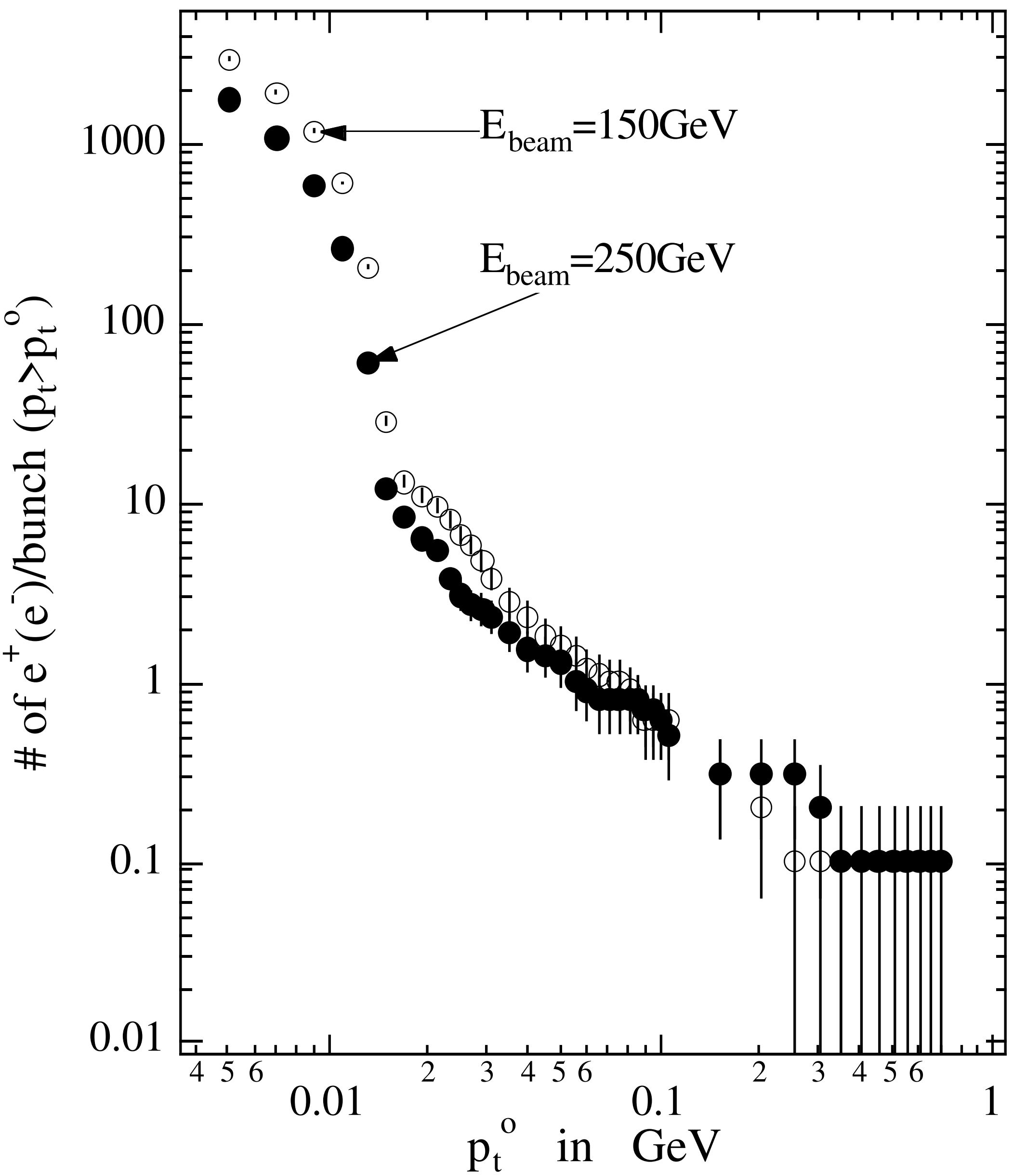

Figure 4: Pair yield/bunch crossing as a function of P_t° for $\theta_e > 0.15$ at JLC-I(c-band).

Table 1: Characteristics of JLC-I

E_{beam} (GeV) Band	150 S	150 C	150 X	250 S	250 C	250 X
L (cm^{-2}sec^{-1}) $\times 10^{33}$	3.5	6.6	3.2	4.8	11.	6.3
L (cm^{-2}bunch^{-1}) $\times 10^{29}$	15.3	6.1	2.4	17.5	10.	4.7
rep. rate (Hz)	50	150	150	50	150	150
number of bunches	46	72	90	55	72	90
bunch separation	5.6ns	2.8ns	1.4ns	5.6ns	2.8ns	1.4ns
$N_{e^\pm}$/bunch $\times 10^{10}$	1.56	1.0	0.63	1.30	1.0	0.63
σ_x (nm)	335.	335.	335.	301.	260.	260.
σ_y (nm)	3.92	3.92	3.92	3.04	3.04	3.04
σ_z (μm)	80.	80.	85.	80.	80.	67.
β_x (mm)	10.	10.	10.	10.	10.	10.
β_y (μm)	100.	100.	100.	100.	100.	100.
D_x	0.21	0.13	0.090	0.13	0.13	0.071
D_y	18.0	11.5	7.7	13.0	11.5	6.1
disruption angle: $\theta_\circ$ (mrad)	0.88	0.57	0.35	0.49	0.44	0.27
crossing angle: ϕ_c (mrad)	11.0	10.4	9.0	7.3	8.0	7.2
$\langle\Upsilon\rangle$	0.14	0.093	0.059	0.23	0.19	0.15
Υ_{max}	0.47	0.32	0.19	0.78	0.70	0.51
energy loss (δ) (%)	7.0	3.5	1.7	9.0	7.0	4.0
n_γ	1.7	1.1	0.74	1.6	1.4	0.91
A	1.3	0.95	0.74	1.0	0.93	0.66
$1.65 \times P_t^{max}$ (MeV) at θ =0.15	26.9	17.2	10.3	22.9	18.2	13.2
R_{mask} (cm)	9.0	5.7	3.5	7.7	6.1	4.4
L_{mask} (m)	0.60	0.38	0.23	0.51	0.41	0.29
$\eta_{mask}(L_Q = 2.5\text{m}) \times 10^{-4}$	6.0	1.9	0.60	3.9	2.2	1.0
total energy deposits(GeV) and e's/bunch						
ΣE_e(no θ_e cut) $\times 10^5$	1.8	0.60	0.17	5.8	3.0	0.91
ΣN_e(〃) $\times 10^4$	6.2	2.0	0.62	7.0	3.9	1.3
$\Sigma E_e(\theta_e > .005) \times 10^4$	13.	4.0	0.55	11.	5.8	1.3
ΣN_e(〃) $\times 10^4$	5.4	1.7	0.49	5.1	2.8	0.96
$\Sigma E_e(\theta_e > .050) \times 10^2$	5.4	4.9	0.94	21.	9.2	2.2
ΣN_e(〃) $\times 10^3$	8.0	5.7	1.0	11.	9.4	3.2
number of hits(e's)/bunch in $\lvert\cos\theta_e\rvert < 0.9$						
$r = 2$ cm	429.4	117.8	63.1	350.2	100.4	81.6
	(188.5)	(21.1)	(5.8)	(69.8)	(34.4)	(11.1)
$r = 5$ cm	76.8	7.3	124.	51.7	21.7	23.3
	(14.6)	(4.7)	(2.8)	(10.9)	(6.8)	(2.9)
$r = 30$ cm	2.3	1.1	0.	1.4	0.3	0.3
	(1.0)	(0.5)	(0)	(0.75)	(0.2)	(0.2)

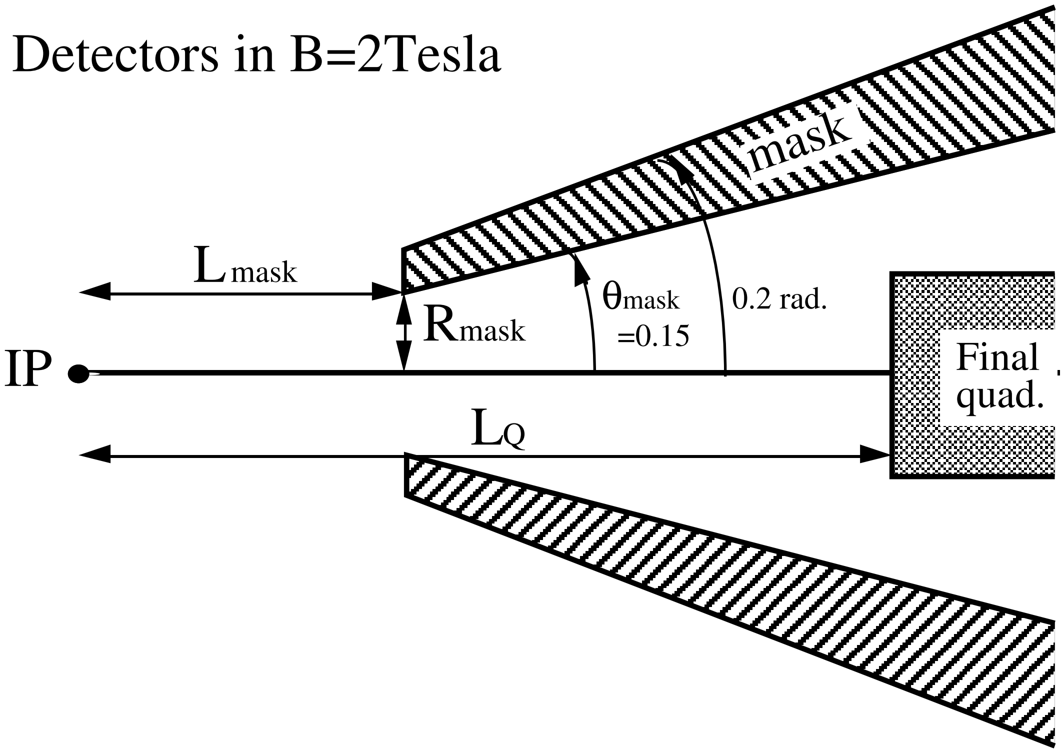

Figure 5: A masking system at the interaction region

this parameter. R_{mask} can be linearly related to a diameter of circular trajectory of a charged track in a solenoidal magnetic field(B), *i.e.* $R_{mask} = p_t^{max}/0.15B$ and B=2Tesla. We determine R_{mask} for the pairs, which comprise a shoulder in Fig.4, to loop inside the mask. There is another important constraint from the solid angle seen by the photons back-scattered at QC1, *i.e.* $\eta_{mask} = R_{mask}^2/4(L_Q - L_{mask})^2 < 1 \times 10^{-3}$, where L_{mask} and L_Q are the distances of the mask and the final focus quadrupole magnet from the interaction point(IP), respectively(Fig.5). The location of the final focus quadrupole magnet has been set to be 2.5 m from IP for the synchrotron radiations to go through QC1 without scattering as mentined in the previous section. The optimized vaues of R_{mask}, L_{mask} and η_{mask} are also listed in Tab.1. With this masking system, the total number of charged particles hitting the outer surface of the mask is less than 10^3/train(72 bunches) as shown in Fig.4.

1.6 Background at the Vertex Detector

In general we can use a beampipe of small radius, e.g. $R_{pipe} \sim$ 1cm, at IP because of no fear of synchrotron radiation as discussed in the previous section. Therefore, a vertex detector can be placed very close to the beam line. In order to estimate the background in the vertex detector, the number of hit points , which the pairs make by traversing the surface of the cylinder of radius R_{vtx} and length $Z_{vtx} = R_{vtx}/\tan\theta_{vtx}$ around the collision point, are plotted as a function of R_{vtx} at $|\cos\theta_{vtx}|$=0.707 and 0.9 in Fig.6(a),(b). Here we assume the helix trajectories of the pairs in the solenoidal magnetic field of 2 Tesla and we allow for the pairs to register multiple hit points without any interaction. The number of hits decreases rapidly as R_{vtx} increases. The hit numbers per bunch crossing are 117.8(21.1) and 100.4(34.4) at R_{vtx}=2cm, $|\cos\theta_{vtx}|$=0.9 for JLC-I(c-band) E_{beam}=150

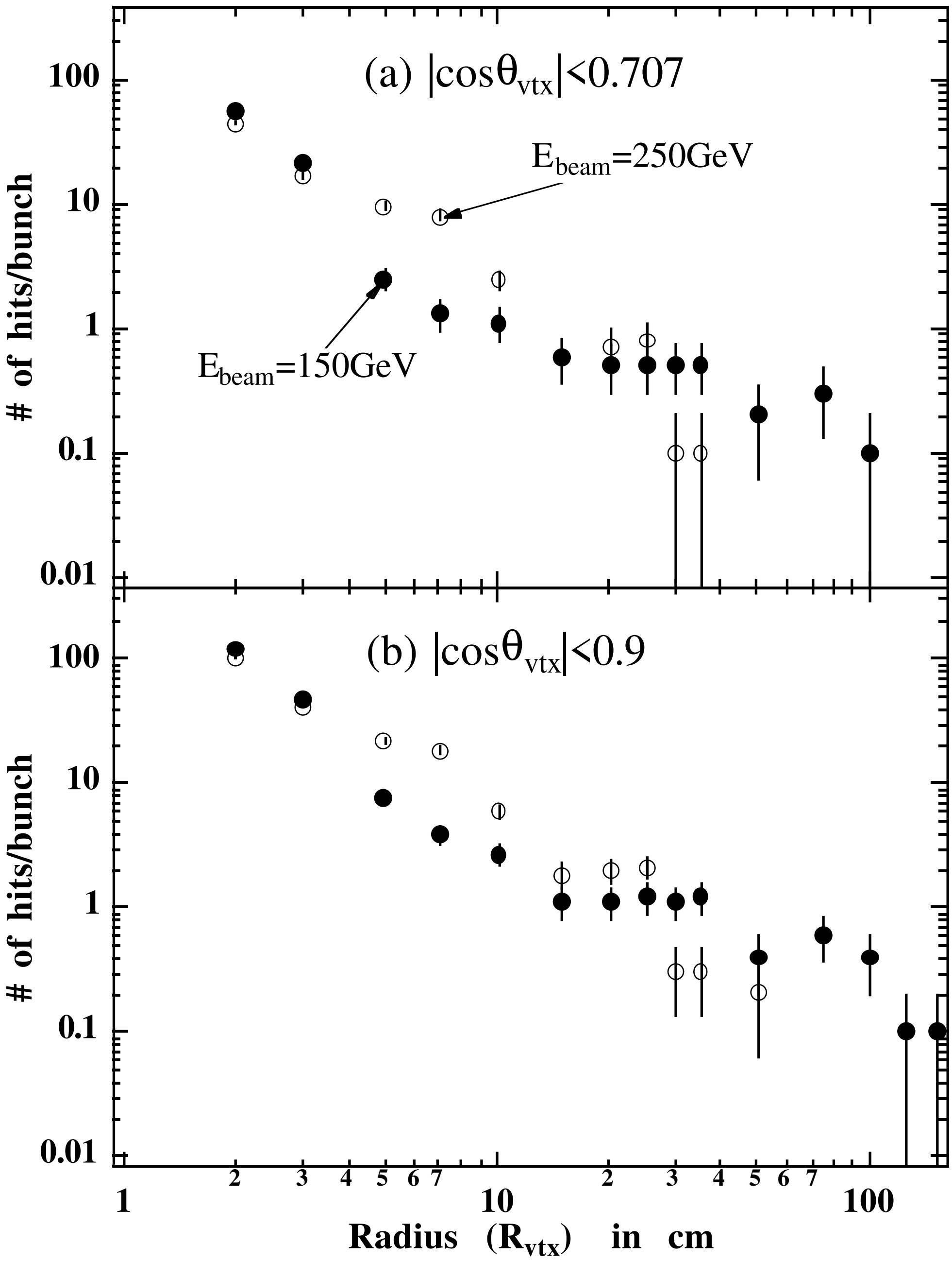

Figure 6: background hits by the pairs in B=2Tesla as a function of radius(R_{vtx}.

and 250GeV, respectively, where values in parenthesis are the number of particles which make hits. The hit numbers have to be multiplied by 72 for a real background estimation because there are 72 bunches/train. This background apparently prevents us from using a gas chamber as the vertex detector in R_{vtx} <10cm. Our CCD(pixel) device is the best detector. The vertex detector also suffers from the secondary photons. Since the number of these photons is on the order of 10^3 per train crossing, the corresponding hit number in the vertex detector is always less than those of the pairs with a few % of the conversion probability of the photons.

References

[1] W.R. Nelson and Y. Namito, MUON89 code for calculation of muon shielding.

[2] E.A. Kushnirenko, "MUON ATTENUATION", presented at FFIR workshop at SLAC, March,1992.

[3] Y. Namito, a detailed simulation is under going.

[4] J.Irwin, "Collimating MegaWatt Micron Sized 250-500 GeV Electron Beams", presented at LC92 at Garmisch-Partenkirchen Germany, July,1992.

[5] K.Yokoya, private communication, and also presented at LC91 at Protvino Russia, September,1991.

[6] W. Lohmann, R. Kopp and R. Voss, "Energy loss of muons in the energy range 1-10000GeV", CERN 85-03, 21 March 1985.

[7] P. Chen and V.I. Telnov, *Phys. Rev. Lett.* **63**, 1796 (1989).

[8] T. Tauchi, K. Yokoya and P. Chen, to be published in *Particle Accelerators* .

[9] T.Tauchi *et al.*, "Background Problem at Interaction Point for an e^+e^- TeV Linear Collider" Presented at the DPF Summer Study on High Energy Physics: Research Directions for the Decade, Snowmass, Colorado, June 25-July 13, 1990, SLAC-PUB-5652.